Numerical Simulation of Two-Dimensional Turbulent Separated and Reattaching Flows Using Reynolds Averaged-Navier Stokes (RANS) Model in Order to Find the Best Mesh and Near-Wall Treatment

Mekhtiche Hamid[1,2], Rebhi Redha[2,3*] and Alliche Mounir[2,3]

[1]Department of Mechanical Engineering, University of Medea, Medea, 26000, Algeria.
[2]Biomaterials and Transport Phenomena Laboratory (LBMPT), University of Medea, Medea 26000, Algeria.
[3]LERM-Renewable Energy and Materials Laboratory, University of Medea, Medea 26000, Algeria.

Received: 13-04-2023 **Accepted**: 25-10-2023 **Published**: 21-11-2023

Abstract

In this work we have studied numerically the flow around a two-dimensional (2D) cubic obstacle using of the technique of computational fluids dynamics (CFD) for a Reynolds number *Re*=40450 based on the bulk velocity and the cannel height. The objective of this study is to evaluate the performance of different turbulence models. For the simulation of turbulent wind flow using the Navier-Stokes equation. We considered five models of turbulence, namely standard k-ε model, realizable k-ε model, RNG k-ε model, standard k-ω model and SST k-ω model. The evaluation is based on the comparison of predicted with those obtained experimentally CEDVAL A1-3, Exp. [33]. The experimental results were produced in a wind tunnel the metrological Institute of Hamburg University. Our main objective in this study is to find the appropriate turbulence model for the simulation of complex flow in the presence of reattachment and separation. Adequate meshes have been used to meet the critical required by each turbulence model.

Keywords: Two-dimensional, Computational fluid dynamics (CFD), Turbulence models, Separation and reattachment.

Tob Regul Sci.™ 2023 ;9(2): 1219-1244
DOI : doi.org/10.18001/TRS.9.2.75

* Author to whom correspondence should be addressed : rebhi.redha@gmail.com

1. Introduction

The flow around surface mounted sharp-edged obstacle has great importance especially in environmental flow and the identification and the study of phenomena that arise in the front and in the wake of obstacles remains a topic of current interest and still remain poorly understood. Because it is a difficult task due to the strong interaction between obstacle walls and the external boundary layer flow and involves many flow interactions such as separation, recirculation and reattachment. Approaching the obstacles, the flow is characterized by undeveloped boundary layers and high turbulence activities, the combined effects of small aspect-ratio, high free-stream turbulence and undeveloped boundary layers give rise to very complex flow structures around the obstacles. With the development of computational (computing) facilities, this topic has received sustained attention over the last decades.

In last decades, numerous studies have sought to understand the separated and reattaching turbulent flow over surface-mounted blocs. By mean of k-ε turbulence model, Murakami and Mochida [1] investigated the 3D flow simulations avec a cubic model. Theirs results showed that the boundary condition for ε at the solid wall had significant influence on the flow field. Also, the top and the lateral boundary conditions can produce undesirable effect near the side wall. Iaccarino et al. [2] studied the numerical simulation the unsteady flow around square cylinder and over a wall-mounted cube with Reynolds averaged Navier-Stokes (RANS) equations and they showed good agreement with experimental data. Steady computations produce an erroneously long wake and the unsteady computations produce the essential physics of three-dimensional. Murakami et al. [3] compare the k-ε and the large-eddy simulation (LES) with the results of wind tunnel experiments. Their results produced by k-ε model revealed significant differences compared with those from wind tunnel tests but the LES model provides a good agreement. Lakehal and Rodi [4] studied by numerical simulations of the flow around a cube (3D) placed in a developed channel flow. The models using wall functions cannot reproduce the details of the complex flow structures near the ground however using the two-layer approach, the results are much improved. Maurizi [5] compared the behaviors of three versions of k-ε closure model implemented in PHONICS software with measured data from the wind tunnel experiment. The RNG turbulence model is generally better than the other, giving à partial justification of the good results for the mean flow. Cheng et al. [6] comparing LES approach and RANS (k-ε) approach, using three types of sub-grid model. They found that the flow structure in the proximity of a cube is captured by both the LES and RANS approaches. However, LES was found to give a better overall quantitative agreement with the experimental data than RANS. Murakami el al. [7] have compared the computational results obtained using Reynolds Averaged-Navier Stokes (RANS) k-ε and large-eddy simulation LES turbulence models with the results of wind tunnel experiments. Salim et al. [8] found that LES significantly improves the flow prediction results as compared to RANS models. Lien et al. [9] showed that the non-linear k-ε turbulence model,

unlike the standard k-ε model, can reproduce with qualitative and quantitative agreement the flow features in the disturbed turbulent flow field through and over the building array. They estimate that the fail of the standard k-ε model is a result of the excessive turbulence energy production due to normal straining. Schmidt and Thiele [10] numerical simulation of turbulence models DNS, LES and RANS on unsteady flow around a square cylinder. The main objective of this study is to evaluate the performance of DES turbulence model compared to the LES and RANS models on a coarse mesh. The results demonstrate that DES is able to capture the most dominant flow patterns like LES, while RANS only gives an only a poor representation of the unsteady flow phenomena. Garcia Sagrado et al. [11] have performed numerical and experimental investigations of pollutant dispersion in a 2D street canyon. The experimental results it has been checked that increasing the height of the downstream building decreases the pollutant concentration in the street. The recirculating bubble inside the street canyon blocks the smoke from going out of the street, helping it to stay trapped in the corners of the street. Also, they found that the realizable k-ε model has been found the more accurately predicts the reattachment length after the step. Trepea [12] studied the influence of Reynolds number and the ratio h/H (obstacle height to channel height) on the reattachment length. Castro [13] studied the influence of the length reattachment on the laminar boundary-layer. The results indicate that for ($0.34<\delta/H<0.8$) decrease the length reattachment at the same time (δ/H), (δ/H, and the ratio of the thickness boundary layer thickness on the block height). Seeta Ratnam and Vengadesan [14] studied the performance of turbulence models to predict the flow heat transfer on a cubic obstacle. The calculation is performed using five turbulence models, standard k-ε, low-Reynolds number k-ε, non-linear k-ε, standard k-ω and improved k-ω to solve the closure problem. The results showed that the improved k-ω model gives a better agreement with the experimental study and the non-linear k-ε model gives a better prediction compared to low-Reynolds number and standard k-ε models. Vardoulakis et al. [15] carried out an evaluation of four computational fluids dynamics (CFD) codes (CHENSI, MIMO, VADIS and Fluent) on the prediction of the flow around an isolated and a tandem of two surface-mounted cubes using the k-ε model. Although the codes reproduced reasonably well the general flow patterns around two surface-mounted cubes of different characteristics, all four codes over-estimated the turbulent kinetic energy generated in the impingement region near the upwind wall of the cubes. Comparing k-ε models variants Wang and Huang [16] showed that the RNG k-ε model and Chen-Kim k-ε have much better ability to predict the characteristics of the vortex structure and flow separation than the standard k-ε model. Sedighi and Farhadi [17] numerical study of the turbulent flow over wall-mounted cube in a channel by large eddy simulation LES and Reynolds number varies from 1000 to 40000. They show that the flow with higher Reynolds number has a shorter reattachment length and by increasing the Reynolds number turbulent intensity and Reynolds stresses increase at the center of the vortexes and sides of the cube respectively. Tominaga and

Stathopoulos [18] studied the accuracy of prediction of flow and dispersion around a cubic building using various k-ε models (standard k-ε model, RNG k-ε model, k-ε model with Launder and Kato modification and k-ε realizable). The numerical results were compared with wind tunnel data. The RNG model showed general agreement with the experiment; however, all models underestimate the concentration diffusion. In a similar study, Lateb et al. [19] found that found that the realizable k-ε turbulence model yielded the best agreement with wind tunnel results for the lowest stack height, while for the highest stack height, the RNG k-ε turbulence model provided greater concordance with experimental results. The realizable k-ε model was the only model able to provide the correct trend for the concentration distribution in the lower region between the two buildings; however, none of the models reproduced the trend in the upper regions. Ariff et al. [20] have studied for dealing with turbulent flow over a surface-mounted cube using the wall y^+ for low Reynolds number. The calculation is performed using five turbulences models are used to solve the closure problem, the standard k-ε, standard k-ω, Reynolds stress model (RSM), Spalart-Allmaras (SA) and renormalization group (RNG) k-ε. The numerical results are compared with experimental data. The author noticed that, the mesh resolving the long-law is sufficiently accurate without incurring additional cost. RSM turbulence model best predicts the flow separation region above the cube whereas the standard k-ε performs better in the flow reattachment and recovery region. Yong et al. The same authors Ariff et al. [21] to resolve the viscous sub layer and buffer region due to the comparatively lower Reynolds number. Köse and Dick [22] by a numerical studied the flow around a cubic building in an atmospheric boundary layer. The results of the numerical simulation are compared with experimental data for the different types of turbulence models, steady state RANS, hybrid RANS/LES and LES. The outcome is that the Implicit LES (ILES) method is the most accurate for coarse grid simulations. An analysis to evaluate the performance of the various non-linear k-ε models for the prediction of the wind flow around an isolated high-rise building in a turbulent boundary layer carried out by Shao et al. [23]. They found that all models reproduce a vortex behind the building during instable calculations. However, the best model (Craft model) slightly over predicts the reattachment length on building roof. The other two non-linear models produce large roof re-circulation vortexes, which extend over the entire roof without attachment. The near-wall treatment and inlet boundary profiles effect on the prediction of flow and dispersion around an isolated building studied by Ai and Mak [24]. They showed that the inlet conditions obtained by fitting the k profile predict flow and dispersion better than that for u profile. Also, they observed that the use of the two-layer model to solve the near-wall viscous sublayer clearly improves the prediction of flow and dispersion. Aliane et al. [25] studied the influence of the Reynolds number and the non-dimensional (obstacle height to cannel height) on the reattachment length for the two-dimensional flow around two models of obstacles, rectangular block obstacle and rounded rectangular obstacle. Cheng and Yang [26] proposed a modified version of k-ε model through modification of the damping function of eddy viscosity that

incorporates the effect of wall proximity in the near the wall region and the effect of non-equilibrium away from the wall together with the simple model functions in the ε-equation. Meroney et al. [27] compared the Reynolds Stress Model (RSM) and standard and Re-Normalized Group (RNG) k-ε turbulence models with wind tunnel test results, and found that the RSM produced more realistic results than the other two k-ε models.

From the previous discussion, it can be seen that the CFD has become a more accessible tool due to the continued progress of modeling studies and the rapid increase of computational resources. However, from the foregoing published literature it seems that the results are varied, confuses sometimes contradictory. Separated flows are significantly affected by the presence of walls, where the viscosity-affected regions have large gradients in the solution variables and accurate presentation of the near-wall region determines successful prediction of separated-reattachment turbulent flows. Also, it is known that the results of CFD simulations are very sensitive to a wide range of computational parameters such as turbulence constants, and the flow profiles of velocity and turbulence quantities.

In all the numerical simulation the accuracy of the results were dependent on the turbulence models, the near-wall treatment (y^+) applied, convergence criteria, among other solver factors.

The objective of this paper is to present a detailed and careful comparison using different turbulence models in order to find the best mesh and near-wall treatment and adequate turbulence model in predicting separated flow. Real physical inlet boundary conditions, that simulate the experimental situations, are chosen for velocity profile and turbulence proprieties. The turbulence models used are: standard k-ε model, realizable k-ε model, RNG k-ε model, standard k-ω model and SST k-ω model.

2. Mathematical formulation of the problem

The governing equations for incompressible fluid flow based on the Reynolds-Averaged Navier-Stokes (RANS) as follows:

$$\frac{\partial \overline{u}_i}{\partial x} = 0 \tag{1}$$

$$\overline{u}_j \frac{\partial \overline{u}_i}{\partial x_j} + \overline{u_j^{'} \frac{\partial u_i^{'}}{\partial x_j}} = \overline{f}_i - \frac{1}{\rho}\frac{\partial \overline{P}}{\partial x_i} + \upsilon \frac{\partial^2 \overline{u}_i}{\partial x_j^2} + S_i \tag{2}$$

$\overline{u}_i$ and $u_i^{'}$ are the mean and fluctuating parts of the velocity component u_i in the x_i-direction, respectively, P is the mean pressure, ρ is the density, υ is the kinematic viscosity, and S_i is the momentum sink defined for the fluid zone demarcated as porous media in order to model the tree crowns. Appearance of the fluctuations associated with turbulence have consequences on the time-averaged Navier-Stokes equations where the velocity fluctuations give rise to additional stresses in the fluid, the so-called Reynolds stresses, $\rho\overline{u_i^{'}u_j^{'}}$ which need to be modeled in order to mathematically close the problem.

3. Turbulence models

No single turbulence model can be universally applied to simulation. Some consideration must be taken when choosing a turbulence model including; physics encompassed in the flow, level accuracy and computational resources available several turbulence transport model will be examined and discussed in this section. Both the standard k-ε model, realizable k-ε model, RNG k-ε model, standard k-ω model and SST k-ω model were tested.

3.1 Standard k-ε turbulence model

This original model was initially proposed by Launder and Spalding [28]. The turbulent kinetic k and its rate of dissipation ε, for this model are obtained by the flowing equations.

$$\frac{\partial}{\partial t}(\rho k)+\frac{\partial}{\partial x_i}(\rho k u_i)=\frac{\partial}{\partial x_j}\left[\left(\mu+\frac{\mu_t}{\sigma_k}\right)\frac{\partial k}{\partial x_j}\right]+G_k+G_b-\rho\varepsilon-Y_M+S_K \quad (3)$$

$$\frac{\partial}{\partial t}(\rho \varepsilon)+\frac{\partial}{\partial x_i}(\rho \varepsilon u_i)=\frac{\partial}{\partial x_j}\left[\left(\mu+\frac{\mu_t}{\sigma_\varepsilon}\right)\frac{\partial \varepsilon}{\partial x_j}\right]+C_{1\varepsilon}\frac{\varepsilon}{k}(G_k+C_{3\varepsilon}G_b)-C_{2\varepsilon}\rho\frac{\varepsilon^2}{k}+S_\varepsilon \quad (4)$$

where G_k represents the generation of turbulent kinetic energy the arises due to mean velocity gradient expressed by $G_k=-\rho\overline{u_i'u_j'}(\partial u_j/\partial x_i)$. The modelulus of mean rate-of-strain tensor S, is defined as $S=\sqrt{2S_{ij}S_{ij}}$. The turbulent (or eddy) viscosity at each point is related to the local values of turbulent kinetic energy and its dissipation rate by;

$$\mu_t=\rho C_\mu\frac{k^2}{\varepsilon} \quad (5)$$

The dilation dissipation term, Y_M which accounts for turbulence from compressibility effects is defined as $Y_M=2\rho\varepsilon M_t^2$. The model is constants are $\sigma_k=1.0,\sigma_\varepsilon=1.3,C_{1\varepsilon}=1.44,C_{2\varepsilon}=1.92,C_\mu=0.09.$

3.2 Realizable k-ε turbulence model

The realizable model by Shih [29] in the most recently developed of the three k-ε variation and futures two main differences from the standard k-ε model. In terms of the improved changes by Shih [29], the transport equations become.

$$\frac{\partial}{\partial t}(\rho \varepsilon)+\frac{\partial}{\partial x_i}(\rho \varepsilon u_i)=\frac{\partial}{\partial x_j}\left[\left(\mu+\frac{\mu_t}{\sigma_\varepsilon}\right)\frac{\partial \varepsilon}{\partial x_j}\right]+\rho C_1 S\varepsilon-C_2\rho\frac{\varepsilon^2}{k+\sqrt{\nu\varepsilon}}+C_{1\varepsilon}\frac{\varepsilon}{k}C_{3\varepsilon}G_b+S_\varepsilon \quad (6)$$

Similar to the previous variations of the k-ε model, the turbulence viscosity is determined by the formula given below; however, it produces different results as C_μ is not constant. where $C_\mu=\frac{1}{A_0+A_s(kU^*/\varepsilon)}$, where $U^*=\sqrt{S_{ij}S_{ij}+\tilde{\Omega}_{ij}\tilde{\Omega}_{ij}}$ and $\tilde{\Omega}_{ij}=\overline{\Omega}_{ij}-\varepsilon_{ijk}\omega_k-2\varepsilon_{ijk}\omega_k$. The constant A_0 and A_s are defined as A_0=4.04, $A_s=\sqrt{6}\cos\phi$; where $\phi=\frac{1}{3}\cos^{-1}\left(\sqrt{6}\frac{S_{ij}S_{jk}S_{ki}}{\tilde{S}^3}\right)$,

$\tilde{S} = \sqrt{S_{ij}S_{ij}}$, $S_{ij} = \frac{1}{2}\left(\frac{\partial u_j}{\partial x_i} + \frac{\partial u_i}{\partial x_j}\right)$. It has been show that C_μ is a function in the mean strain and rotational rates. The standard value of C_μ=0.09 is found to be the solution of equation (2.32) for an inertia sub layer in the equilibrium boundary layer. The constants $C_{1\varepsilon}, C_{2\varepsilon}, \sigma_k$ and σ_ε have been determined by Shih [29] are defined as follows. $C_{1\varepsilon} = 1.44, C_2 = 1.9, \sigma_k = 1.0$ and $\sigma_\varepsilon = 1.2$.

3.3 RNG k-ε turbulence model

Similar to the standard k-ε model the RNG model was derived from the instantaneous Navier-Stokes equations, except is uses a technique called renormalization group theory described by Yakhot and Orszag [30]. The transport equations as follows:

$$\frac{\partial}{\partial t}(\rho\varepsilon) + \frac{\partial}{\partial x_i}(\rho\varepsilon u_i) = \frac{\partial}{\partial x_j}\left[\alpha_\varepsilon \mu_{eff}\frac{\partial \varepsilon}{\partial x_j}\right] + C_{1\varepsilon}\frac{\varepsilon}{k}(G_k + C_{3\varepsilon}G_b) - C_{2\varepsilon}\rho\frac{\varepsilon^2}{k} - R_\varepsilon + S_\varepsilon \qquad (7)$$

The RNG theory uses a scale elimination procedure that defines the effective viscosity given in the following equation: $d\left(\frac{\rho^2 k}{\sqrt{\varepsilon\mu}}\right) = 1.72\frac{\nu}{\sqrt{\hat{\nu}^3 - 1 + C_\nu}}d\nu$ where $\hat{\nu} = \mu_{eff}/\mu$ and C_ν is a constant equal approximately to 100. The constant C_μ derived using the RNG theory and found to be 0.0845, the other constant $\sigma_\varepsilon = 0.719, C_{1\varepsilon} = 1.42, C_{2\varepsilon} = 1.68$.

3.4 Standard k-ω turbulence model

The standard k-ω turbulence model developed by Wilcox [31] that was formulated to better compute low-Reynolds number effects, compressibility and shear flow spreading. The standard model is an empirical based model with transport equations for turbulent kinetic energy (k) and its specific dissipation rate (ω). The transport equations used for Wilcox's model are as follows.

$$\frac{\partial}{\partial t}(\rho k) + \frac{\partial}{\partial x_i}(\rho k u_i) = \frac{\partial}{\partial x_j}\left[\left(\mu + \frac{\mu_t}{\sigma_k}\right)\frac{\partial k}{\partial x_j}\right] + G_k - Y_k + S_k \qquad (8)$$

$$\frac{\partial}{\partial t}(\rho\omega) + \frac{\partial}{\partial x_i}(\rho\omega u_i) = \frac{\partial}{\partial x_j}\left[\left(\mu + \frac{\mu_t}{\sigma_\omega}\right)\frac{\partial \omega}{\partial x_j}\right] + G_\omega - Y_\omega + S_\omega \qquad (9)$$

where G_ω is generation of ω which are defined in the exact manor as the k-ε model. The turbulence viscosity is defined using a damping coefficient α^*: $\mu_t = \alpha^*(\rho k/\omega)$. The low-Reynolds number correlation is obtained from this coefficient α^* which damps the turbulent viscosity. This coefficient is given by $\alpha^* = \alpha^*_\infty\left(\frac{\alpha^*_0 + (\mathrm{Re}_t/R_k}{1 + (\mathrm{Re}_t/R_k}\right)$ where $\mathrm{Re}_t = \rho k/\mu\omega, R_k = 6, \alpha^*_0 = B_i/3$ and $\beta_i = 0.072$. For the high-Re from of the standard k-ω model $\alpha^* = \alpha^*_\infty = 1$, the term for the dissipation of k due to turbulence, Y_k is defined as

$Y_k = \rho\beta^* f_{\beta^*} k\omega$ and the term for the dissipation of ω due to turbulence Y_ω is defined as $Y_\omega = \rho\beta f_\beta k\omega^2$.

3.5 SST k-ω turbulence model

The shear stress transport k-ω model, it was developed by Menter [32] using the standard k-ω model and a transformed k-ε model. Similar to the standard k-ω model, the transport equation for k and ω are slightly modified and are given by:

$$\frac{\partial}{\partial t}(\rho k)+\frac{\partial}{\partial x_i}(\rho k u_i)=\frac{\partial}{\partial x_j}\left[\left(\mu+\frac{\mu_t}{\sigma_k}\right)\frac{\partial k}{\partial x_j}\right]+\tilde{G}_k-Y_k+S_k \tag{10}$$

$$\frac{\partial}{\partial t}(\rho\omega)+\frac{\partial}{\partial x_i}(\rho\omega u_i)=\frac{\partial}{\partial x_j}\left[\left(\mu+\frac{\mu_t}{\sigma_\omega}\right)\frac{\partial \omega}{\partial x_j}\right]+G_\omega-Y_\omega+D_\omega+S_\omega \tag{11}$$

where $\tilde{G}_k$ represents the generation of turbulent kinetic energy the arises due to mean velocity gradient, $\tilde{G}_k = \min(G_k, 10\rho\beta^* k\omega)$. The term for the production of ω, G_ω defined as $G_\omega = \alpha G_k/\upsilon_t$. The turbulence viscosity is computed in a different way from that used in the standard model and is given by $\mu_t = \frac{\rho k}{\omega}\frac{1}{\max\left[1/\alpha^*, SF_2/a_1\omega\right]}$. Blending function have been add to the SST model to ensure that the model equations behave appropriately in both near wall and for field zones. $\sigma_k = \frac{1}{(F_1/\sigma_{k,1})+(1-F_1)/\sigma_{k,2}}$, $\sigma_\omega = \frac{1}{(F_1/\sigma_{\omega,1})+(1-F_1)/\sigma_{\omega,2}}$, with $F_1 = \tanh(\Phi_1^4), F_2 = \tanh(\Phi_2^4)$. The cross-diffusion term, D_ω blends the standard k-ε model and the standard k-ω model and is defined as: $D_\omega = 2(1-F_1)\rho\sigma_{\omega,2}\frac{1}{\omega}\frac{\partial k}{\partial x_j}\frac{\partial \omega}{\partial x_j}$. The constant specific to the SST k-ω model are defined as $\sigma_{\omega,1}=2.0, \sigma_{\omega,2}=1.168, \sigma_{k,1}=1.176, \sigma_{k,2}=1.0, a_1=0.31.$

4. Methodology and computational Details

The geometry of the flow under consideration is shown in Fig.1. A fully turbulent flow with Reynolds number were considered. The *x*-axis aligned along the inlet flow and *z*-axis perpendicular to the cube axis. The computational domain dimensions are 18.7*H* and 7*H* for length and height, respectively. The location of the inflow and outflow boundaries is arrived and they are placed at the locations as shown in Fig. 1. Such distances are chosen to ensure that the inlet length has no effect on the results and the recirculation zone is inside the computational domain and the outflow has no effect upon the physical variables investigated.

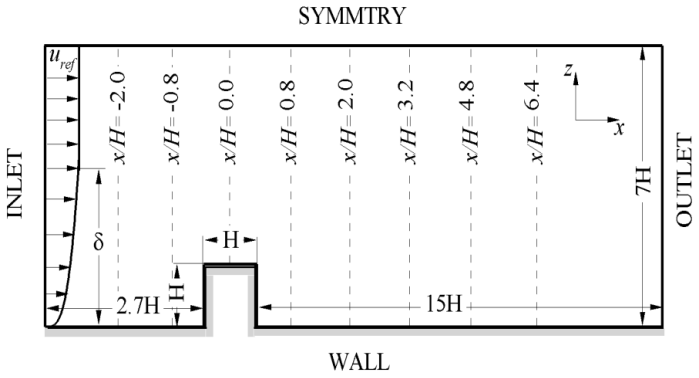

Figure 1. Schematic representation of the modeling domain.

Computational domain is bounded by the floor of the wind tunnel and obstacle "Wall", for which a non-slip condition is applied, $u=v=w=0$. At the top of the domain the symmetry line is chosen to satisfy the zero-stress boundary condition. At the inlet, a profile fitted the experimental data of CEDVAL A1-3, Exp. [33], (Metrological Institute of Hamburg University) is imposed Eq. (12). The parameters used in experimental data are as follow: the depth of the atmospheric boundary layer equal to 3H, the free stream velocity u_0 ($z=\delta$) equal to $5ms^{-1}$ and the roughness length $z_0=10^{-3}m$. The experimental parameters of wind tunnel used by CEDVAL are given in Tab 1. The fitted profile presented with experimental data in Fig 2.

$$u = ay^b \tag{12}$$

with $a=e^B$, $b=A$, A and B are constants (A = 3.00547 and B = 1.69502).

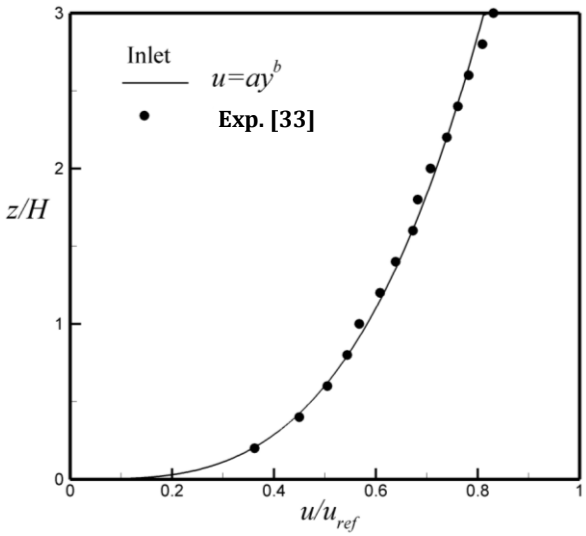

Figure 2. Velocity profile at the inlet.

The turbulent kinetic energy k was calculated from the fluctuating velocity values measured in the wind the wind tunnel CEDVAL A1-3, Exp. [33].

$$k = \frac{1}{2}\left(\overline{u'^2} + \overline{w'^2}\right) \tag{13}$$

Dissipation of turbulence ε (square cubic meter per second) is defined by the following relation.

$$\varepsilon = C_{\mu}^{3/4} \frac{k^{3/2}}{\kappa z} \tag{14}$$

where z is the channel height, and κ is the Von Karman constant $\kappa = 0.4$.

Turbulent frequency ω is calculated by

$$\omega = \frac{k}{\upsilon(\mu_t / \mu)} \tag{15}$$

The wall y^+ is a non-dimensional distance similar to local Reynolds number. In the context of CFD, it is used to describe how coarse or fine a mesh is for a particular flow. It determines whether the influences in the wall-adjacent cells are laminar, transitional or turbulent, hence indicating the part of the turbulent boundary layer that is resolved (ANSYS CFX). It is described as:

$$y^+ = \frac{u^* y}{\upsilon} \tag{16}$$

where y is the height from the wall to the mid-point of the wall-adjacent cells, υ is the kinematic viscosity and u^* is the friction velocity.

At the outlet, zero gradients are imposed for all independent variable except for the pressure where zero pressure was applied.

Table1. The parameters measures CEDVAL A1-3, Exp. [33]: the roughness of the walls z_0, Reference velocity u_{ref}, the reference height z_{ref}, and the height of cube H.

	z_0(m)	u_{ref} (m/s)	z_{ref}(m)	H (m)
CEDVAL A1-3, Exp. [33]	0.001	5	0.750	0.125

ANSYS CFX code, based on Finite Volume Method (FVM), was used for the solution of the conservation equations that governing the problem (Navier-Stokes and turbulence quantities) for all of turbulence models used in this study. Calculation are performed using the k-ε and k-ω variants models, e.g., standard k-ε model, realizable k-ε model, RNG k-ε model, and standard k-ω and SST k-ω model.

The pre-processor ICEM associated with ANSYS CFX is used for the construction of the computational domain and grid generation. A Cartesian structured grid non uniform in the tow direction X and Y is used. A special attention was paid to the generation, in particular near wall treatment. Because the grid adaptation it is a major step in validating the model for future analysis. In all cases the choice of grid mesh configuration, with respect to the turbulence model selected, was based the value of the non dimensional distance from the wall y^+ calculated using

Eq. 16. The grid was adjusted multiple times based on the y^+ values of near wall cells until the y^+ values were within the limiting range. The computation domain is divided to five blocks of non-uniform structured mesh as shown in Fig 3.

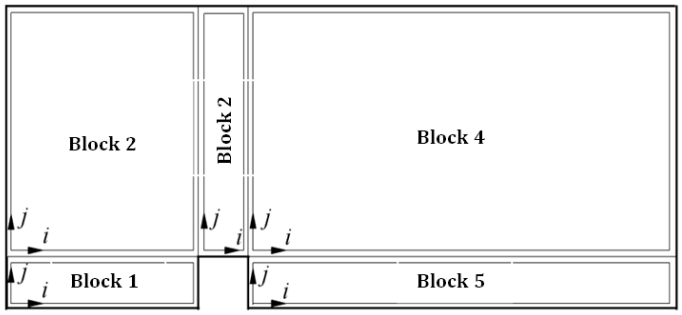

Figure 3. The topology of the mesh.

After the first node near the wall, the mesh is refined to capture high gradient of velocity, pressure and turbulence quantities in the vicinity of the wall. For each turbulence model used, a grid independence study was carried to find the mesh that allows a compromise between desired accuracy and solution cost in time and memory. For this purpose, three mesh sizes of significantly different grid resolution has been tested for the four turbulence models studied, named coarse, mean refined and dense mesh as detailed in Table 2.

Table 2. The numbers of the nodes in the different blocks of the mesh.

	Models: k-ε, RNG k-ε, SST k-ω and k-ω		
	Coarse	Mean refined	Dense
Block 1	101×76	151×101	201×151
Block 2	101×101	151×151	201×201
Block 3	76×101	101×151	151×201
Block 4	201×101	301×151	401×201
Block 5	201×76	301×101	401×151

The three-mesh tested are illustrated in Fig 4. For turbulence models that use wall functions equation (k-ε, RNG k-ε), the first cell is placed in the fully turbulent (log-law region) just after the buffer layer which satisfy the condition $y^+ \approx 30$. For SST k-ω and k-ω turbulence models, the first cell is placed in the viscous layer, very close to the wall at $y^+ \approx 1$ to capture the viscous flow effects. Hence, the height of the near wall cell was 0.04H for the k-ε family and 0.0004H for k-ω family. This because, for the first case the flow in the viscous sublayer and buffer layer does not have to be resolved and wall functions are used instead to calculate all quantities. However, for the second case, the flow in the viscous sub-layer will be resolved and no extra wall functions are introduced.

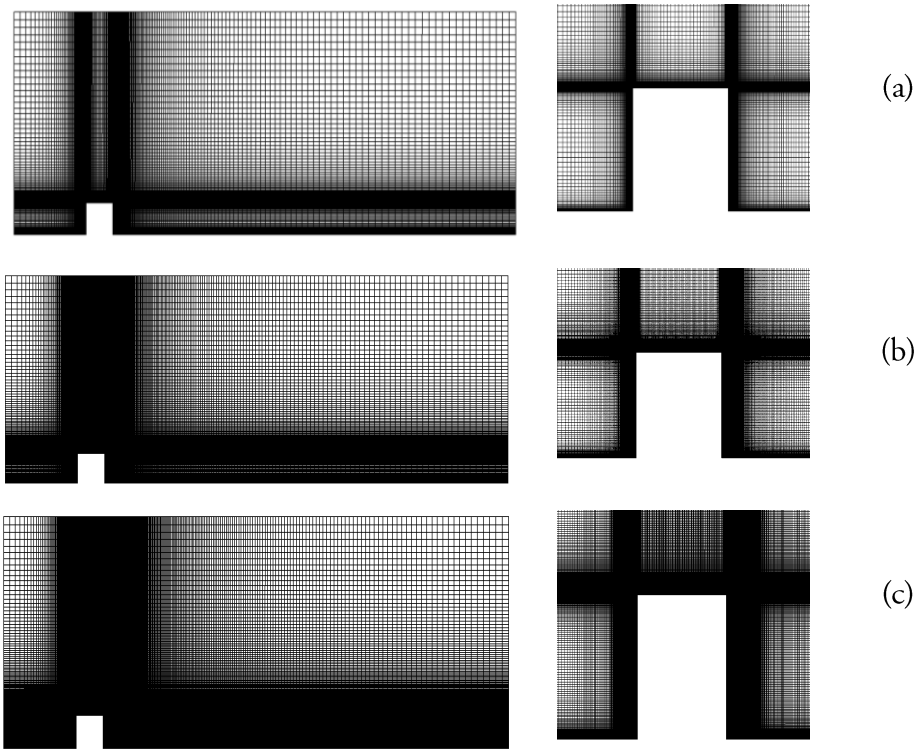

Figure 4. Distribution of meshes: (a) Coarse, (b) Mean refined and (c) Dense.

The y^+ near wall evolution obtained by standard k-ε model and SST k-ω model for the considered mesh are presented graphically in Fig 5. The sharply drop and spikes in wall y^+ are expected due to the presence of the obstacle (obstruction) in the main way flow direction.

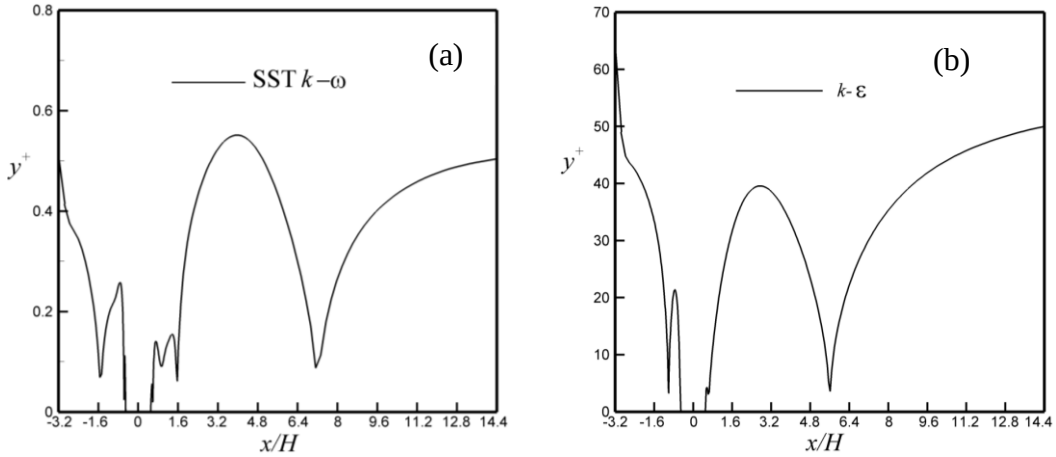

Figure 5. y^+ evolution for turbulence models: (a) k-ε and (b) SST k-ω.

5. Results and discussion

The experimental dataset used for comparisons were obtained from measurement in wind tunnel for the flow around a rectangular building placed in the neutral boundary layer at the metrological institute of Hamburg university, Exp. [33]. All computations are carried out in the steady state conditions and calculation. The solution is considered to be converged when all

residuals are less than or equal to this prescribed value for each variable. A sample of convergence history is illustrated in Fig 6.

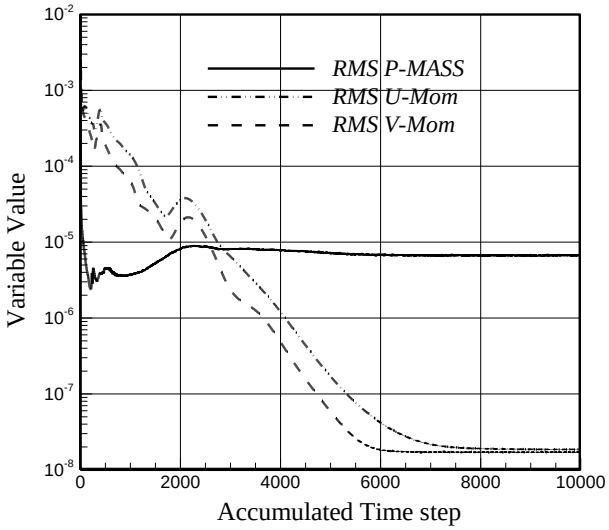

Figure 6. Convergences.

In order to assess the grid sensitivity of the results presented, additional calculations on a progressive refined grid were carried out. In each case, the grid was obtained by multiplying the number of points by a factor of 1.5, in both *x* and directions. The comparison between the results obtained with coarse, fine and dense grid, using SST k-ω model, is reported in Fig 7. It can be shown that, in terms of mean flow velocity profiles, the solution convergence has been reached and the solution becomes independent of the mesh sizes over the mesh called fine mesh. Further mesh refinement was tested and not presented for brevity.

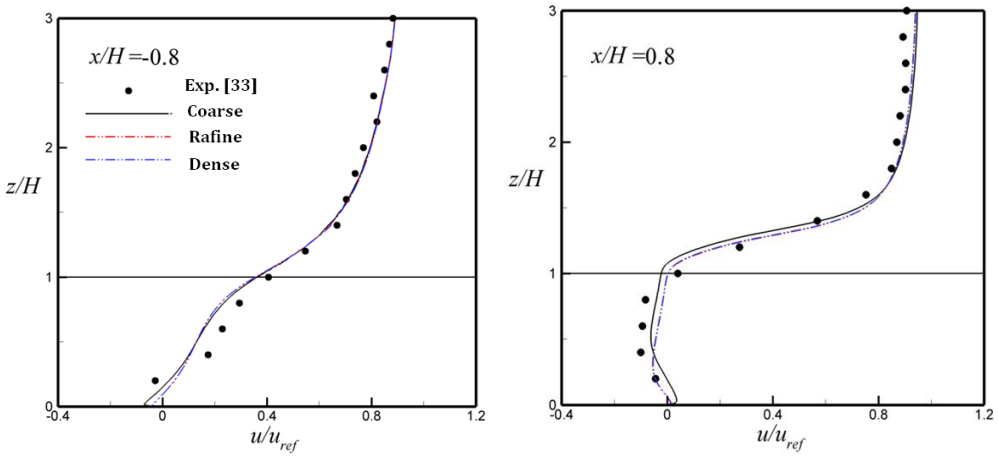

Figure 7(a). Comparison of velocity profiles *u* in the symmetry line *x/H* (-0.8 and 0.8) using SST k-ω model.

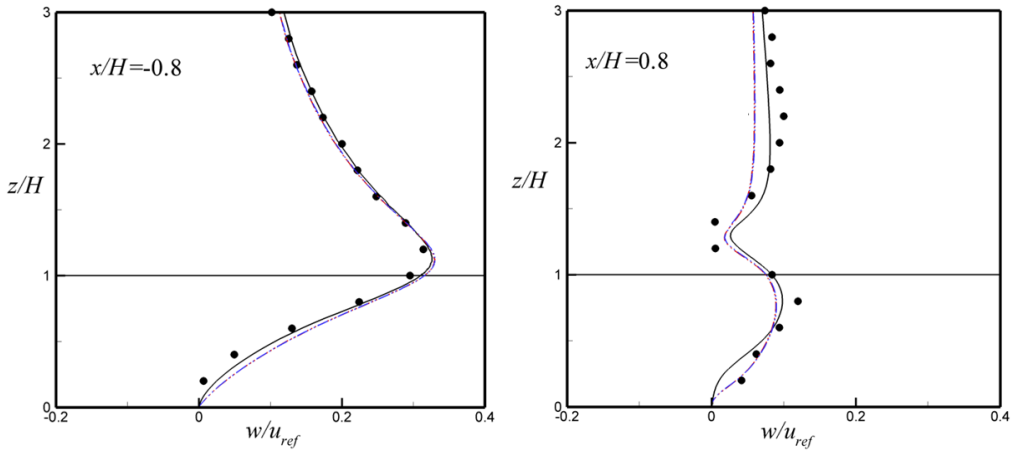

Figure 7(b). Comparison of velocity profiles *w* in the symmetry line *x/H* (-0.8 and 08) using SST k-ω model.

Figure 8 shows the profiles of the two velocity components at different sections upstream, above and downstream obstacle obtained with the four turbulence models (standard k-ε, realizable k-ε, RNG k-ε, k-ω and SST k-ω) plotted with experimental data. It can show that, away in the upstream obstacle, the profiles of u-velocity component obtained with the different turbulence models are comparable and they are close to the experimental measurement, except the flow predicted with k-ω where the *u* velocity component is underestimated long a small portion near the ground (Fig 8a). Approaching obstacle, all models slightly underestimate the u-velocity as compared to the wind-tunnel results, Exp. [33], at a level about a half of obstacle height; however, the profile is well correctly predicted elsewhere. The regions where the turbulence models begin fails to estimate the correct velocity correspond to the onset of vortex recirculation which formed at the frontal base of the obstacle. The rapid change to the high-pressure gradient, caused by the stagnation point, prevents to capture adequately the flow field, in this region. Above the obstacle, the RNG k-ε and the SST k-ω predict more accurately the u-velocity profile especially near the wall where a small size bubble separation occurs, as we will disuse later. Just downstream of the obstacle, a slight deviation from the experimental data were observed at about the mid height obstacle. Above the obstacle roof, the RNG k-ε and the SST k-ω show better agreement with experimental data. Away in the downstream, practically all models predict recovery of flow. For the v-velocity component (Fig 8b), it is correctly predicted only by the two turbulence models RNG k-ε and the SST k-ω, above the obstacle. As expect this region correspond to a small bubble recirculation which lead a vertical flow. Because of its low magnitude, the *v*-velocity component is well predicted elsewhere in whole domain.

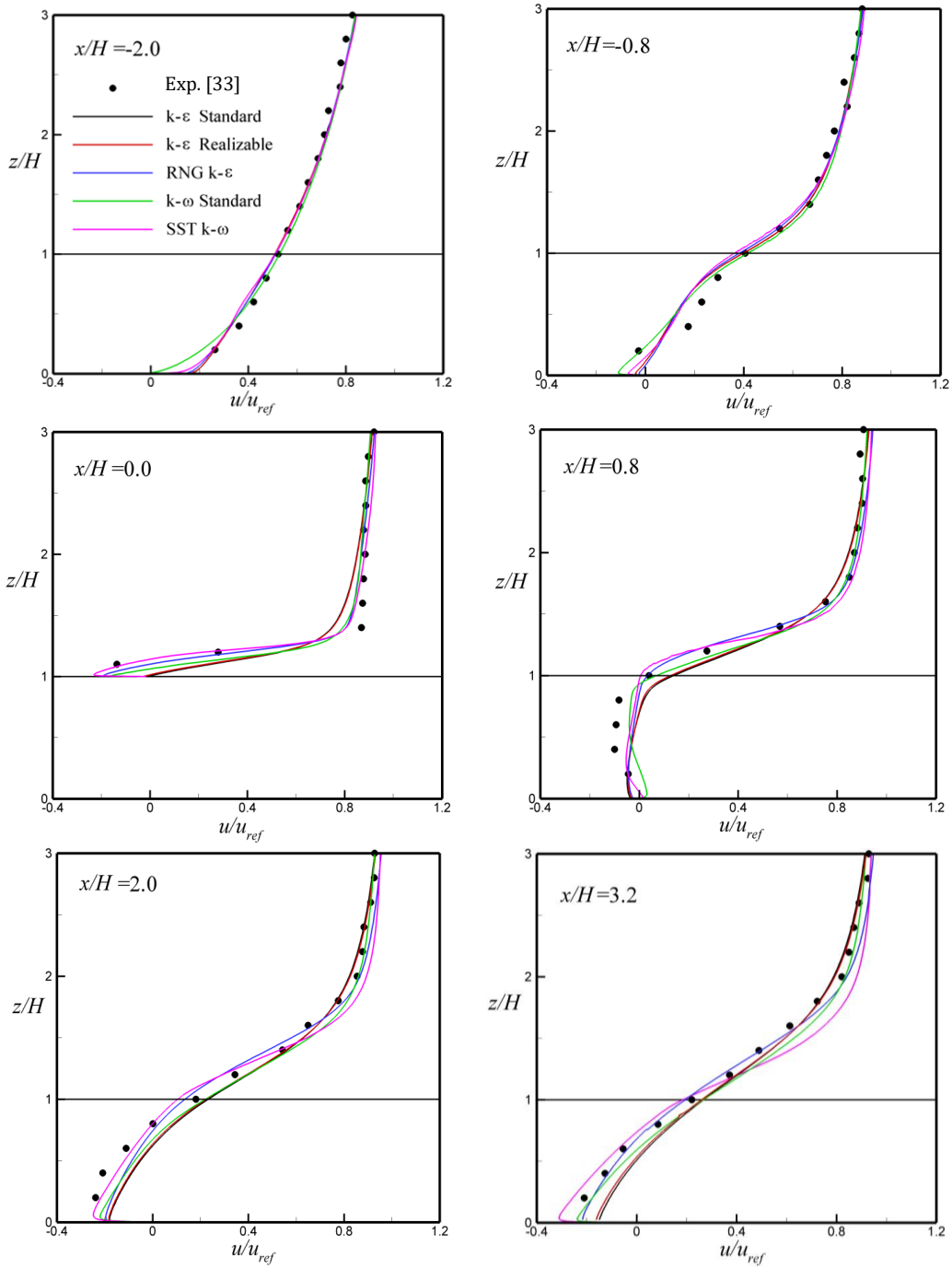
x/H =-2.0
Exp. [33]
k-ε Standard
k-ε Realizable
RNG k-ε
k-ω Standard
SST k-ω
x/H=-0.8
x/H =0.0
x/H=0.8
x/H =2.0
x/H=3.2
z/H
u/u_ref

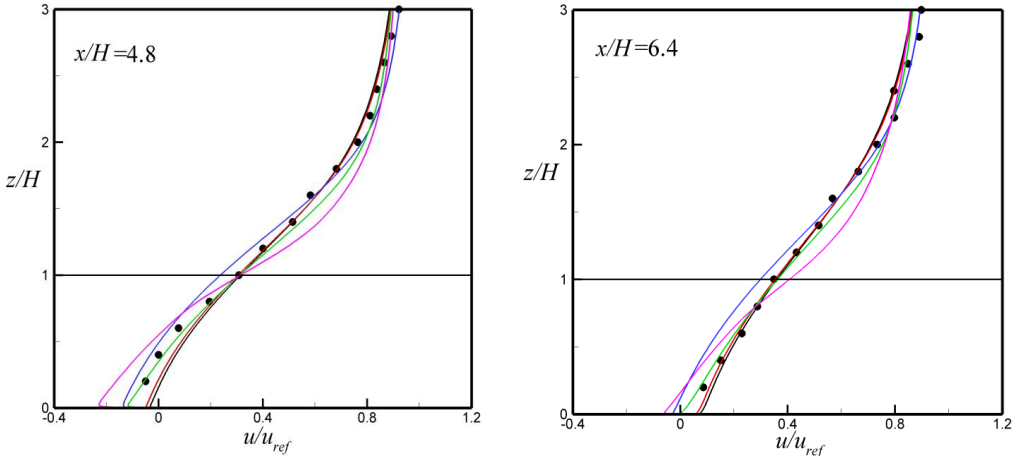

Figure 8(a). Comparison of the predicted velocity u/u_{ref} with those of the experimental data by CEDVAL A1-3, Exp. [33], at different locations.

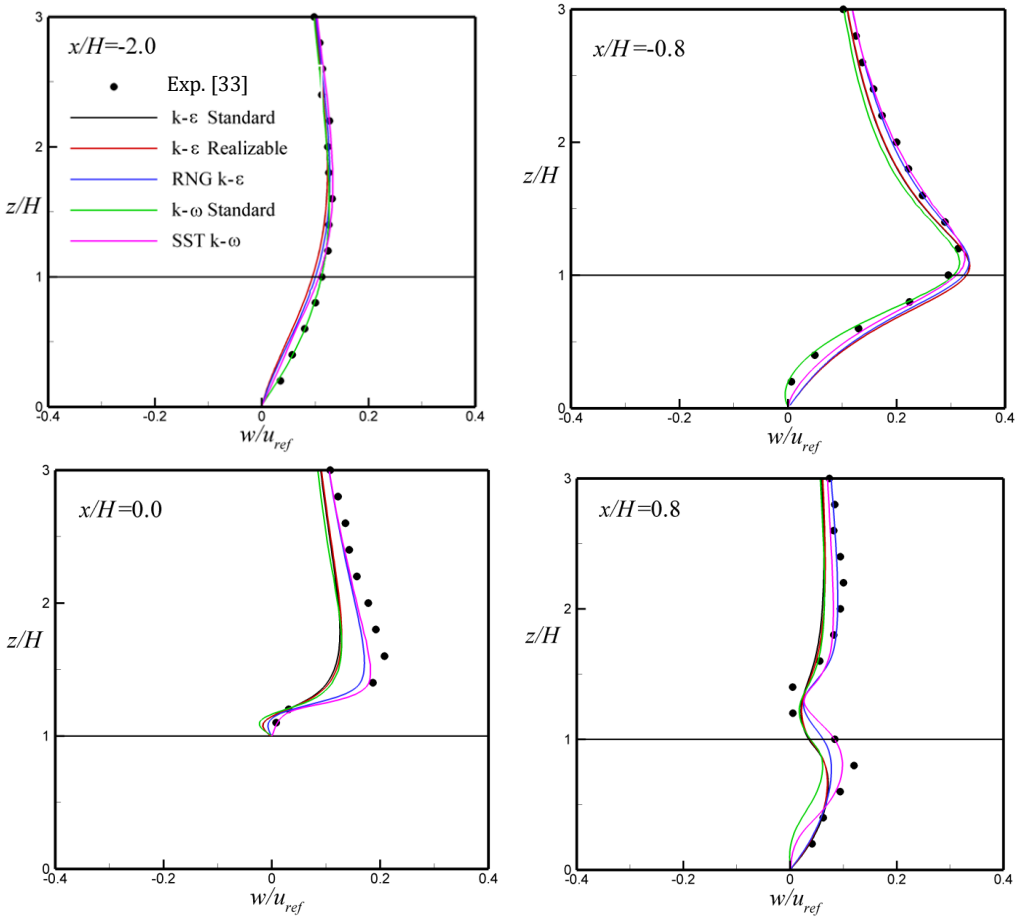

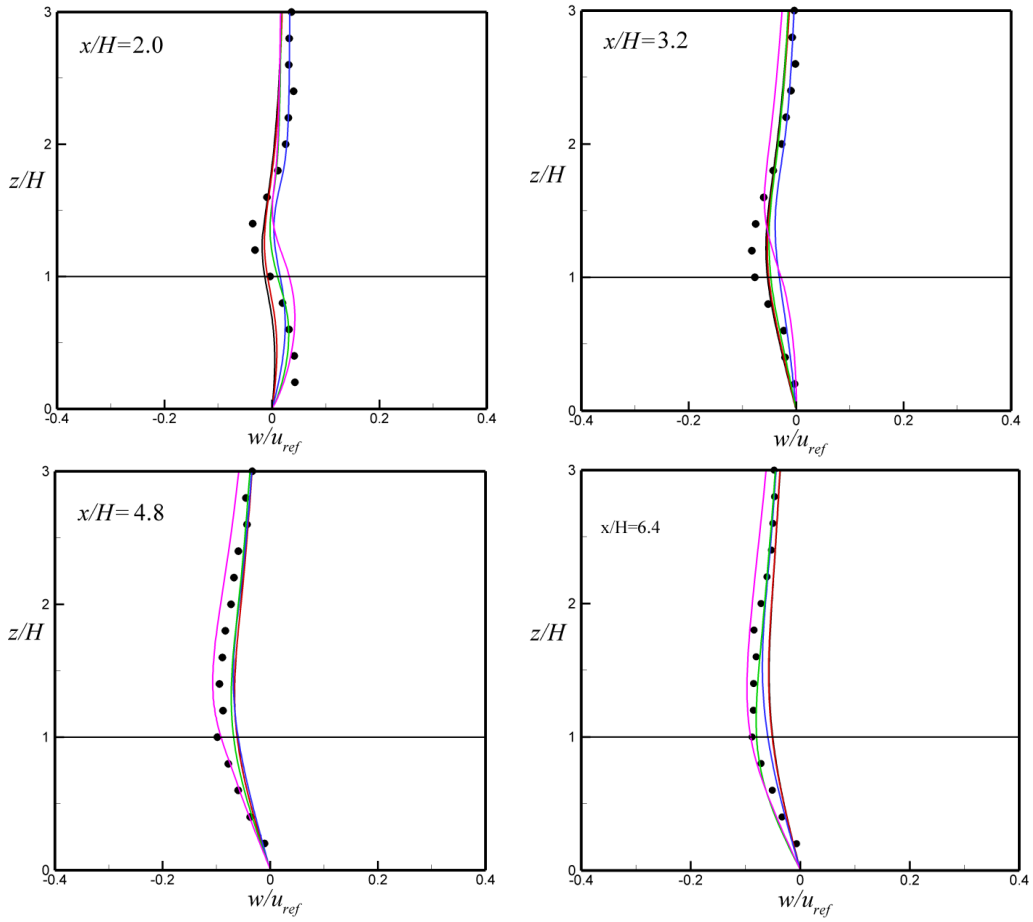

Figure 8(b). Comparison of the predicted velocity w/u_{ref} with those of the experimental data by CEDVAL A1-3, Exp. [33], at different locations.

Streamlines and pressure distribution (back ground color) are used to visualize the flow structure in the whole domain. The flow filed obtained by the five turbulence models is depicted in Fig 9. In general, in term of global qualitative form all models can predict the flow structure formed by separation recirculation and reattachment. It can be shown that, with the five-turbulence model used, the general flow features and the overall prediction of the front, top and rear vortex modes are quite similar, although some differences are visible. The description of the common behavior is as follow: approaching the obstacle, the flow stagnates at the windward surface of the obstacle. Some fluid flows towards the bottom and forms a small vortex at the frontal base of the obstacle. The fluid flowing towards the roof separates at the windward edge of the roof forming a small recirculation bubble at the top of the obstacle. At the leading edge, the flow separating creates wake of highly recirculating flow, behind the obstacle, that is dominated by an arch-shaped vortex in the wake region. For pressure evolution, to satisfy the momentum equation the static pressure increases significantly in the front part of the recirculation zone and decreases above the obstacle.

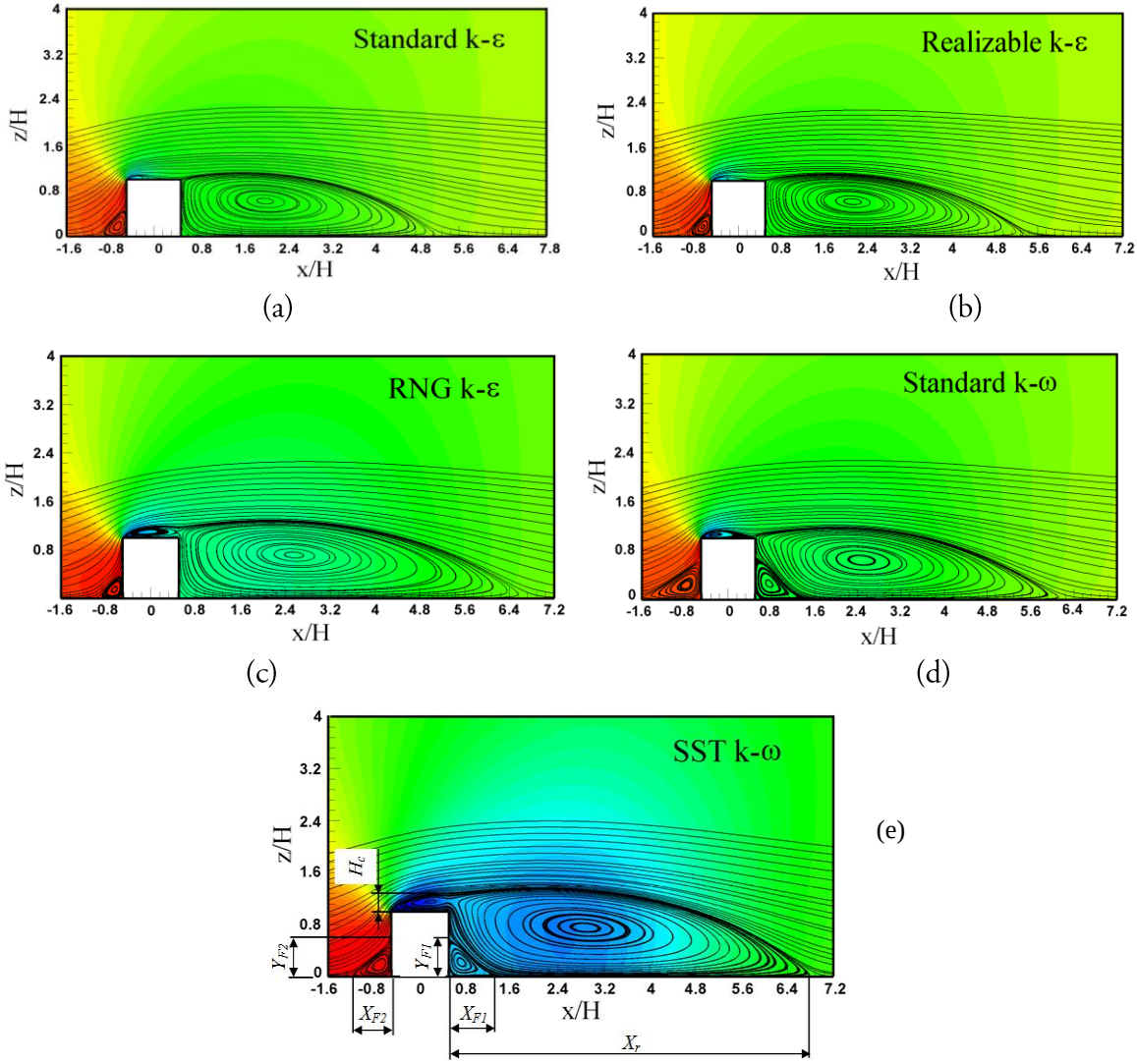

Figure 9. Comparison of streamlines in symmetry plane *z/H* = 0.

Figure 10(a) show vector plot velocities measured along the centerline *xz* plane of the wind tunnel CEDVAL A1-3, Exp. [33], while Fig 10b show corresponding velocities obtained by numerical simulation using SST k-ω turbulence model. The flow structure obtained by SST k-ω consistent with the physics of the turbulent flows obtained in wind tunnel under the same conditions.

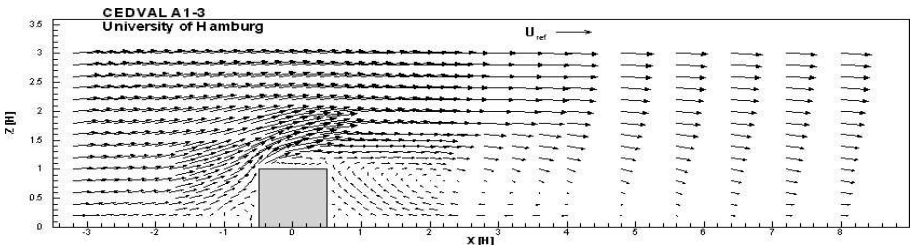

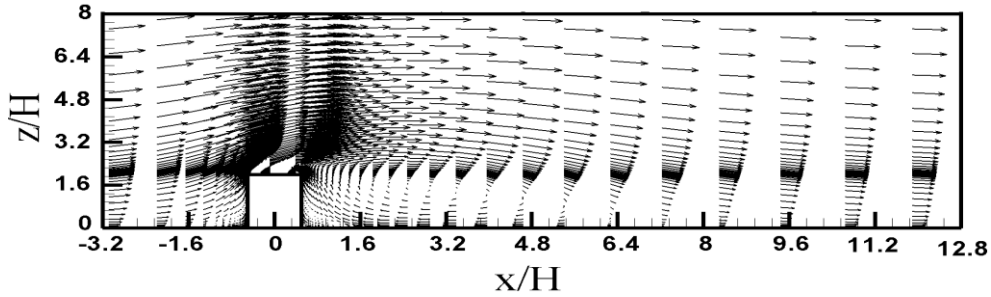

(b)

Figure 10. Comparison of vectors plot between (a) CEDVAL A1-3 dataset, Exp. [33], and (b) simulation numerical turbulence model SST k-ω.

The prediction of separation and reattachment points can be considered as a fundamental test of the capability of turbulence models in separated flow simulations. From Fig 9 and Table 3, it can show that the separation point of the vortex in the upstream obstacle is underpredicted by the standard k-ε and Realizable k-ε models, the underprediction is more pronounced in the RNG k-ε model. However, it is slightly overpredicted by SST k-ω model. The prediction given the standard k-ω is so far from the experimental results. The stagnation point is well predicted by the Realizable k-ε and SST k-ω models. For the flow separation formed by the bubble above the obstacle, a flow reattachment is observed in the results obtained the k-ε standard, k-ε realizable and k-ω turbulence models, however in the experimental results as well as in those predicted by RNG k-ε and SST k-ω turbulence models this reattachment is not obtained and the recirculation situated downstream is extend over the block face. The same phenomenon is obtained using DNS turbulence model (Hattori and Nagano [34]). The k-ω family models results in a very different wake structure than the k-ε family models. Indeed, the decomposition of the recirculation zone formed downstream obstacle into two contra-rotating, main and secondary vortexes, is well predicted only by the k-ω family models and give better agreement the experimental measurements. The presence of this secondary circulation is consistent in the experimental measurement by CEDVAL A1-3, Exp. [33], and therefore it's seems to be characteristic of the real flow. The flow recirculation zone behind the obstacle is overpredicted resulting in a larger reattachment length which consequently under predicts flow recovery by RNG k-ε, k-ω and SST k-ω models. However, the reattachment length is underpredicted by the standard k-ε model. A similar under prediction of flow recovery is obtained by Lakehal and Rodi [4] using various versions of the k-ε model and Shah and Ferziger [35] using more computationally expensive LES model. The Realizable k-ε estimates fairly the flow recovery but it fall to predict the secondary vortex as well as the velocity profiles the recirculation zone. In our opinion, the overprediction of the reattachment length by SST k-ω model can attributed to the 2D assumption used in this study. The work of Martinuzzi and Tropea [36] showed that this length can extend up to 7.4 for a large aspect ratio. Also, they found that the flow becomes quasi 2D for an aspect ratio (*w/h*) over than 25. It can be concluded that, although the SST k-ω model

overestimates the flow reattachment length, it can fairly predict all recirculation zones, e.g., upstream, above and downstream obstacle zone, better than all other models as shown in Fig 9 and Table 3.

Table 3. Characteristic lengths of the flow field for the CEDVAL A1-3, Exp. [33], and turbulence models.

Model	The characteristic lengths						
	(X_R/H)	(X_{F1}/H)	(Y_{F1}/H)	(X_{F2}/H)	(Y_{F2}/H)	(Xc/H)	(Hc/H)
Exp. [33]	5.00000	0.60000	0.50000	-0.50000	0.60000	….	0.25000
Standard k-ε	4.72480	….	….	-0.45856	0.51672	0.06037	0.37017
Realizable k-ε	4.92824	….	….	-0.45424	0.50848	0.06763	0.42081
RNG k-ε	6.23328	0.11876	0.11684	-0.41448	0.41646	0.95888	0.16832
Standard k-ω	6.13088	1.12780	0.71323	-1.84248	0.72120	0.94480	0.12412
SSTk-ω	6.70096	1.05068	0.60118	-0.87408	0.51976	….	0.26496

The results of the effect Reynolds number *Re* on the reattachment X_R/H, separation X_{F1}/H and stagnation X_{F2}/H lengths obtained by SST k-ω are presented in Fig. 11 and Table 4. In transitional flow, the reattachment length increases with increasing in Reynolds number. In fully developed turbulent flow, increasing in *Re* results in reduction of the reattachment length. The reduction of the recirculation zone is due to that the higher flow velocity results in higher wall shear stress and hence yields a shorter reattachment length.

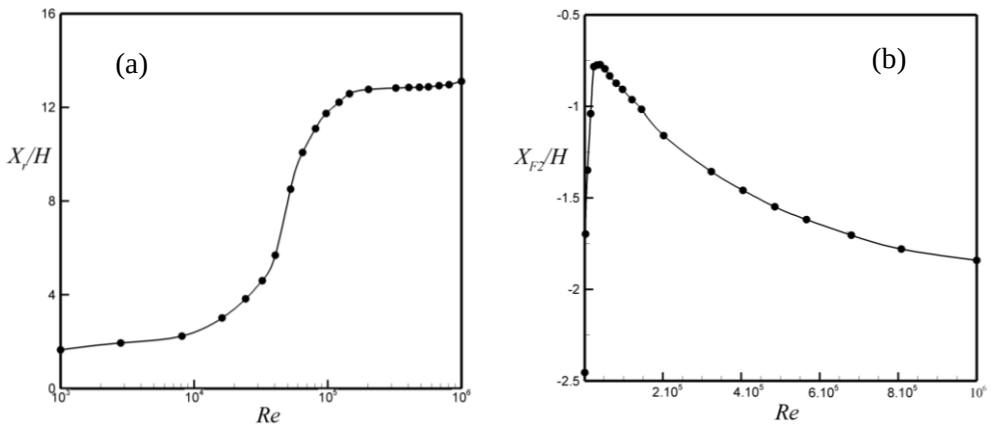

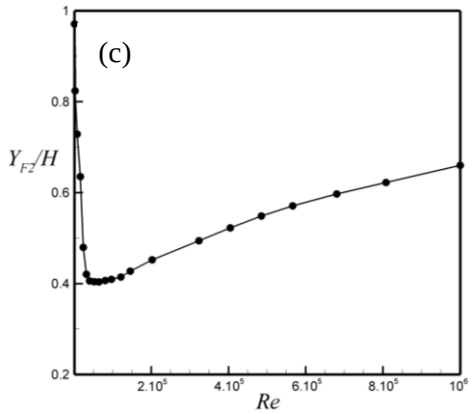

Figure 11. Correlation of: (a) reattachment (X_R/H), (b) separation (X_{F1}/H) and (c) stagnation (X_{F1}/H) with Reynolds number *Re*.

Table 4. The characteristic lengths for the SST k-ω model for different values of Reynolds number *Re*.

Reynolds (*Re*)	The characteristic lengths for Model SST k-ω		
	Reattachment (X_r/H)	Séparation (X_{F2}/H)	Stagnation (Y_{F2}/H)
1000	1.650215	-2.454624	0.970720
24270	3.823832	-0.782656	0.479625
40450	5.686824	-0.772480	0.405992
80900	11.09080	-0.873920	0.406474
121351	12.21424	-0.963312	0.414392
202252	12.76440	-1.159464	0.451948
404504	12.84552	-1.458640	0.522210
680471	12.92356	-1.704050	0.596895
808171	12.97002	-1.779664	0.622204
1000000	13.11222	-1.841232	0.660010

In this section, we consider the case of the two-dimensional flow around in a tilted plan with obstacle at 15°. The investigated geometry show in Fig. 12. The influence of the obstacle height varied from 0.5H to 4.0H on the reattachment length is considered. In the present study, a simulation of the wind flow is carried out using the SST k-ω turbulence model. At the inflow boundaries, measured profiles of the velocity, the turbulent kinetic energy and the turbulent frequency were prescribed.

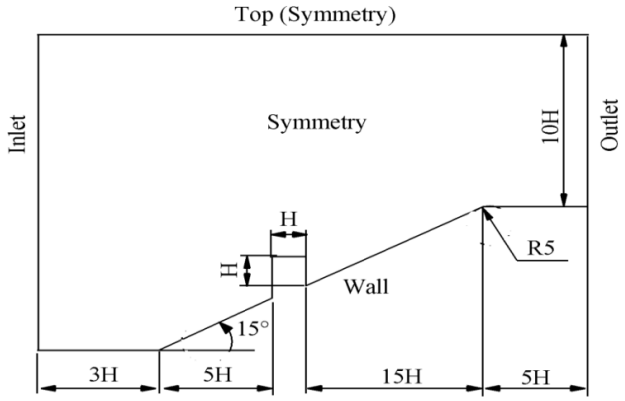

Figure12. Schematic representation of the modeling domain.

The streamlines pressure distributions in the *xz*-plane for different *H* (height obstacle) are shown in Fig 13. Indeed, it is found that the reattachment length X_R and the dimension (X_{F1}, Y_{F1}) of the second recirculation zone (downstream of the obstacle) are presented in Fig 13 and Tab. 5 increases with increasing in the height obstacle (*H*).

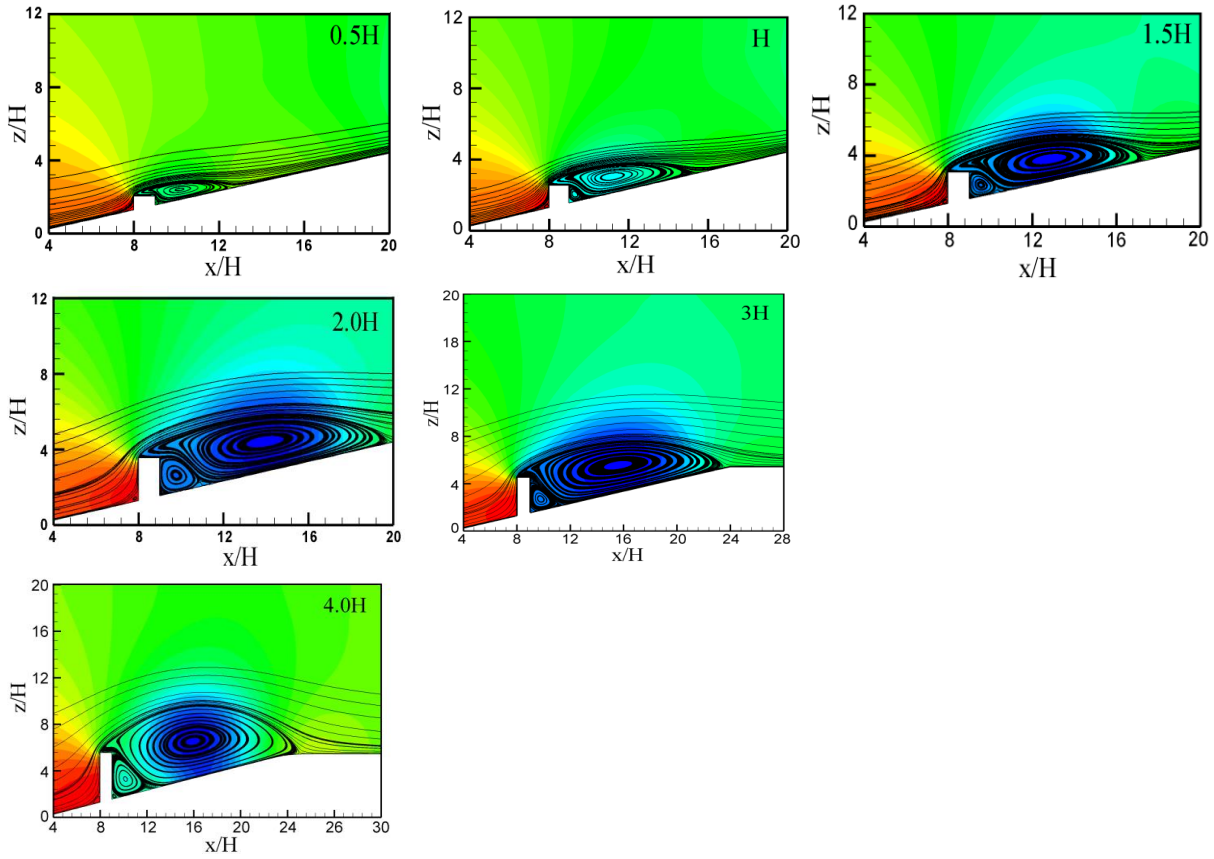

Figure 13. Streamlines in symmetry plane *z/H* for θ=15°.

The effect of the obstacle height varied from 0.5H to 5H on the reattachment length is illustrate in Fig 14 and Table 5. A bird eye view on the results indicate that the characteristic lengths increased with increase of the obstacle height, *H*.

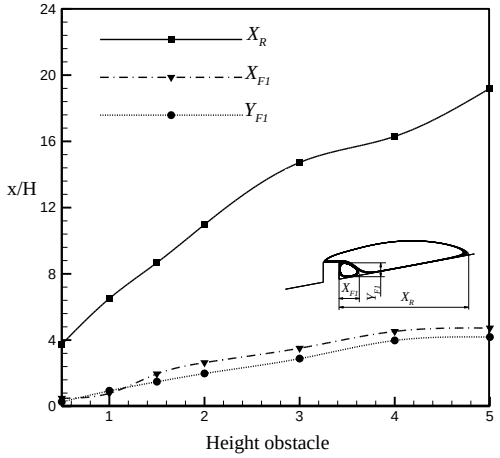

Figure 14. Characteristic lengths of the flow field for tilted plan with obstacle.

Table 5. Characteristic lengths of the flow field for tilted plan with obstacle.

Obstacle height	The characteristic lengths		
	(X_R/H)	(X_{F1}/H)	(Y_{F1}/H)
0.5H	3.7476	0.4854	0.27650
1.0H	6.5073	0.7849	0.94059
1.5H	8.5243	1.9575	1.48873
2.0H	10.976	2.6399	1.98496
3.0H	14.7216	3.6682	2.87035
4.0H	16.2994	4.5241	3.98000
5.0H	19.1986	4.7274	4.18270

6. Conclusion

In this work, a numerical simulation of the turbulent flow around a two-dimensional cubic obstacle (2D) in a channel was performed. To validate the results of the numerical simulation by those in the experimental CEDVAL A1-3, Exp. [33], we considered five models of turbulence (model k-ε standard, model k-ε Realizable, model RNG k-ε, model k-ω and k-ω SST model). Results are obtained for both cases many local Reynolds: 1) for low Reynolds number turbulence models y^+ ~1 and 2) for the turbulence models to many local Reynolds y^+>30.

The results generally indicate a consistent behavior on all models despite that there an acceptable deviation from the set of experimental data. It was also shown that the results of turbulence models of the k-ε family are very different turbulence models of the k-ω family. Indeed, the decomposition of the recirculation zone downstream of the barrier consists of two vortices rotating against, primary and secondary. It is expected that the models of the k-ω family

give better agreement with experimental measurements. The presence of this secondary flow is consistent with the experimental measurement and it seems to be characteristic of the actual flow. It can be concluded that, although the turbulence model SST k-ω overestimates the connecting length of the flow, it may provide enough all-recirculation zones, for example upstream zone, above and below the obstacle, better than all the other models.

For the case tilted plan with obstacle, the increased obstacle height increases the characteristic lengths of the flow field.

References

1. Murakami. S and Mochida. A. (1988). 3-D numerical simulation of airflow around a cubic model by means of the k-ε model. Journal of Wind Engineering and Industrial Aerodynamics, vol. 31, pp. 283-303.
2. Iaccarino. G., Ooi. A., Durbin. B. A and Behnia. M. (2003). Reynolds averaged simulation of unsteady separated flow. Int. J. Heat and Fluid Flow, vol. 24, pp. 147-156.
3. Murakami. S., Mochida. A and Hayashi. Y. (1990). Examining the k-ε model by means of a wind tunnel test and Large-Eddy simulation of the turbulence structure around a cube. Journal of Wind Engineering and Industrial Aerodynamics, vol. 35, pp. 87-100.
4. Lakehal. D and Rodi. W. (1997). Calculation of the flow past a surface-mounted cube with two-layer turbulence models. J. Wind Eng. Ind. Aerodyn, vol. 67&68, pp. 65-78.
5. Maurizi. A. (2000). Numerical simulation of turbulent flows over 2D valleys using three versions of the k-ε closure model. J. Wind Eng. Ind. Aerodyn, vol. 85, pp. 59-73.
6. Cheng. Y., Lien. F. S., Yee. E and Sinclair. R. (2003). A comparison of large Eddy simulations with a standard k-ε Reynolds-averaged Navier-Stokes model for the prediction of a fully developed turbulent flow over a matrix of cubes. J. Wind Eng. Ind. Aerodyn, vol. 91, pp. 1301-1328.
7. Murakami. S., Mochida. A., Hayashi. Y. (1990/91). Numerical simulation of velocity field and diffusion field in an urban area. Energy and Buildings, vol. 15-16, pp. 345-356.
8. Salim. M. S., Cheah. S. C and Chan. A. (2011). Numerical simulation of dispersion in urban street canyons with avenue-like tree plantings: Comparison between RANS and LES. Building and Environment, vol. 46, pp. 1735-1746.
9. Lien. F. S., Yee. E and Cheng. Y. (2004). Simulation of mean flow and turbulence over a 2D building array using high-resolution CFD and a distributed drag force approach. J. Wind Eng. Ind. Aerodyn, vol. 92, pp. 117-158.
10. Schmidt. S and Thiele. F. (2002). Comparison of numerical methods applied to the flow over wall-mounted cubes. Int. J. Heat and Fluid Flow, vol. 23, pp. 330-339.

11. Garcia Sagrado. A. P. G., Beeck. J., Rambaud. P and Olivari. D. (2002). Numerical and experimental modelling of pollutant dispersion in a street canyon. J. Wind Eng. Ind. Aerodyn, vol. 90, pp. 321-339.
12. Tropea. C.D and Gackstatter. R. (1985). The flow over two–dimensional surface-mounted obstacles at low Reynolds numbers. ASME Journal of Fluids Engineering, vol. 107, pp. 489-494.
13. Castro. I. P. (1981). Measurements in shear layers separating from surface-mounted bluff bodies. J. Wind Eng. and Ind. Aero, vol. 7, pp. 253-257.
14. Seeta Ratnam. G and Vengadesan. S. (2008). Performance of two equation Turbulence models for prediction of flow and heat transfer over a wall mounted cube. International Journal of Heat and Mass Transfer, vol. 51, pp. 2834-2846.
15. Vardoulakis. S., Dimitrova. R., Richards. K., Hamlyn. D., Camilleri. G., Weeks. M., Sini. J. F., Britter. R., Borrego. C., Schatzmann. M and Moussiopoulos. N. (2011). Numerical model inter-comparison for wind flow and turbulence around single-block buildings, Environ Model Assess, vol. 16, pp.169-181.
16. Wang. J.S and Huang. Z. (2007). A TVD scheme for incompressible flow coupled with different turbulence models on a ground-mounted square rib-flow. Journal of Hydrodynamics. Ser. B, vol. 19, pp. 743-750.
17. Sedighi. K and Farhadi. M. (2006). Three-dimensional study of vortical structure around a cubic bluff body in a channel. Mechanical Engineering, vol. 4, pp. 1-16.
18. Tominaga. Y and Stathopoulos. D. (2009). Numerical simulation of dispersion around an isolated cubic building: comparison of various types of k-ε models. Atmospheric Environment, vol. 43, pp. 3200-3210.
19. Lateb. M., Masson. C., Stathopoulos. T and Bédard. C. (2013). Comparison of various types of k-ε models for pollutant emissions around a two-building configuration. J. Wind Eng. Ind. Aerodyn, vol. 115, pp. 9-21.
20. Ariff. M., Salim. S.M and Cheah. S.C. Wall y^+ approach for dealing with turbulent flow over a surface mounted cub: part 1-low Reynolds number, Seventh International Conference on CFD in the Minerals and Process Industries CSIRO, Melbourne, Australia 9-11 December (2009a).
21. Ariff. M., Salim. M.S and Cheah. S.C. Wall y^+ approach for dealing with turbulent flow over a surface mounted cub: part 2-High Reynods number, Seventh International Conference on CFD in the Minerals and Process Industries CSIRO, Melbourne, Australia 9-11 December (2009b).
22. Köse. D. A and Dick. E. (2010). Prediction of the pressure distribution on a cubical building with implicit LES. J. Wind Eng. Ind. Aerodyn, vol. 98, pp. 628-649.

23. Shao. J., Liu. J and Zhao. J. (2012). Evaluation of various non-linear k-ε models for predicting wind flow around an isolated high-rise building within the surface boundary layer. Building and Environment, vol. 57, pp. 145-155.
24. Ai, Z.T and Mak. C.M. (2013). CFD simulation of flow and dispersion around an isolated building: Effect of inhomogeneous ABL and near-wall treatment. Atmospheric Environment, vol. 77, pp. 568-578.
25. Aliane. K., Sebbane. O et Houmat. A. (2006). Etude expérimentale de l'écoulement bidimensionnel autour d'un obstacle rectangulaire et un obstacle rectangulaire arrondi. Afrique Science, vol. 2 pp. 285- 299.
26. Cheng, T.S and Yang, W.J. (2008). Numerical simulation of three-dimensional turbulent separated and reattaching flows using a modified turbulence model. Computers & Fluids, vol. 37 (3), pp. 194-206.
27. Meroney, R.N., Leitl, B.M., Rafailidis, S and Schatzmann, M. (1999). Wind-tunnel and numerical modeling of flow and dispersion about several building shapes. Journal of Wind Engineering and Industrial Aerodynamics, vol. 81, pp. 333-345.
28. Launder, B.E and Spalding, D.B. Lectures in Mathematical Models of Turbulence, Academic Press, 1972.
29. Shih, T.H., Liou, W.W., Shabbir, A., Yang, Z., and Zhu, J. (1995). A New-Eddy-Viscosity Model for High Reynolds Number Turbulent Flows-Model Development and Validation. Computers Fluids, vol. 24(3), pp. 227-238.
30. Yakhot, V and Orszag, S.A. (1986). Renormalization Group Analysis of Turbulence: Basic Theory. Journal of Scientific Computing, vol. 1(1), pp. 1-51.
31. Wilcox, D. C. Turbulence Modeling for CFD, DCW Industries, Inc., La Canada, California, 1998.
32. Menter, F.R. (1994). Two-Equation Eddy-Viscosity Turbulence Models for Engineering Applications. AIAA Journal, vol. 32(8), pp. 1598-1605.
33. Leitl. B. (2003). Compilation of experimental data for validation of micro scale dispersion models, http://www.mi.uni-hamburg.de/cedval/
34. Hattori, H and Nagano, Y. (2012). Structures and mechanism of heat transfer phenomena in turbulent boundary layer with separation and reattachment via DNS. international Journal of Heat and Fluid Flow, vol. 37, pp. 81-92.
35. Shah, K.B and Ferziger, J.H. (1997). A fluid mechanicals view of wind engineering: Large eddy simulation of flow past a cubic obstacle. Journal of Wind Engineering and Industrial Aerodynamics, vol. 67-68, pp. 211-224.
36. Martinuzzi, R and Tropea, C. (1993). Flow around surface-mounted, prismatic obstacles placed in a fully developed channel flow. Journal of Fluids Engineering, Transactions of the ASME, vol. 115, pp. 85-92.